Ex vivo Dynamic Imaging of Retinal Microglia using Time-lapse Confocal Microscopy

Jung Eun Lee[1,2], **Katharine J. Liang**[1,2], **Robert N. Fariss**[3], and **Wai T. Wong**[1]

1*Office of the Scientific Director, National Eye Institute, National Institutes of Health, Bethesda, MD, USA*

2*Division of Epidemiology and Clinical Research, National Eye Institute, National Institutes of Health, Bethesda, MD, USA*

3*Biological Imaging Core, National Eye Institute, National Institutes of Health, Bethesda, MD, USA*

Abstract

Purpose—Retinal microglia have been implicated in the pathogenesis of various retinal diseases, but their basic function and cellular phenotype remains incompletely understood. Here, we used a novel *ex vivo* retinal imaging preparation to examine the behavioral phenotype of living retinal microglia in intact tissue and in response to injury.

Methods—Fluorescently-labeled microglia in retinal explants from CX3CR1$^{+/GFP}$ transgenic mice were observed using time-lapse confocal imaging. High spatial and temporal resolution imaging parameters were used to follow dynamic microglial behavior in real time.

Results—Under normal conditions, resting retinal microglia are not static in structure but instead exhibit extensive structural dynamism in their cellular processes. Process movements are highly random in direction, but are balanced to maintain overall cellular symmetry and arbor size. At rest, these exuberant process movements do not however result in overt cellular migration. Following focal laser injury, microglial processes increase significantly in their motility and direct themselves towards the injury site. Microglia rapidly transition their morphologies from symmetrical to being from polarized towards the laser lesion. Microglia also transition from a fixed to a migratory phenotype, translocating through tissue while retaining their ramified morphology.

Conclusions—Retinal microglia normally occupying uninjured tissue display a continuous, dynamic behavior that suggests functions of tissue surveillance and intercellular communication. Microglial behavior is highly regulated by, and immediately responsive to, focal tissue injury and may constitute a therapeutic cellular response to focal laser photocoagulation. *Ex vivo* live imaging in the retina is an experimental approach well suited to the study of dynamic aspects of microglial physiology.

Introduction

Microglial cells are resident immune cells of the central nervous system[1, 2]. Akin to macrophages, microglia play a key role in innate and adaptive immunity, mediating immune tissue protection against infection and neuronal insults.[3] However, they can also be involved in exacerbating tissue damage through neurotoxic and pro-inflammatory effects when fully activated.[4] Unlike brain microglia which have a broad distribution throughout neural tissue, retinal microglia exhibit a stratified distribution correlating to the laminar organization of the retina.[5] In normal adult retina, microglia are largely restricted to the inner retinal layers and

Corresponding author: Dr Wai T. Wong, Office of the Scientific Director, National Eye Institute, National Institute of Health, 7 Memorial Drive, Room 217, Bethesda, Maryland 20892, Tel: (301) 905-7301. Fax: (301) 496-1759. Email: wongw@nei.nih.gov.

are largely absent from the region extending from the outer nuclear layer to Bruch's membrane. [6]

Similar to their counterparts in the brain, retinal microglia have also been implicated in a number of retinal degenerative, inflammatory, and vascular diseases.[7–9] Activated retinal microglia have been found in human histopathological specimens of retinal disease in tissue locations where pathological changes are found.[10–12] Abnormal accumulation and altered morphologies of retinal microglia have also been found in animal models of retinal disease, including retinal detachment[9], retinitis pigmentosa [8, 13] age-related macular degeneration[14, 15], and diabetic retinopathy.[16] In the latter, studies in mouse models[16] and human disease[12] demonstrate that morphological changes in retinal microglia occur early in disease progression, suggesting that these may have a inductive role in causing pathologic neuronal and vascular changes. Numerous studies have demonstrated that microglia, in general, display a multi-faceted array of structural phenotypes that can change markedly depending on the tissue context [17, 18]. These phenotype changes include alterations in cellular morphology, tissue distribution, migratory characteristics, and changes in process structure. These structural phenotypes are thought to reflect different functional modes, enabling microglia to effect different changes in the surrounding tissue [2]. In the retina, characterizations of these microglial phenotypes under normal and disease conditions, and how they reflect on changing microglia function, are not well understood. In addition, how various therapeutic interventions in retinal disorders may cause changes in microglia physiology is also unknown.

In this study, we used a novel *ex vivo* imaging approach to study not only the structure but also the behavior of living retinal microglia in intact tissue. Previous studies have shown that microglia in the cerebral cortex demonstrate structural dynamism in their ramified processes [19, 20] but whether this behavior extends to areas outside the brain, and specifically to the retina, has not been examined. Although recent studies have examined how microglia may accumulate and traffic in the retina *in vivo* over the time scale of hours to days [21], the higher spatial and temporal resolution of our imaging system enables us to follow detailed changes in the structure of individual microglial processes and quantitate process and migration velocities. In addition, our system is amenable to examining changes in microglia behavior under different conditions. Here, we examined changes in microglial behavior before and following focal laser treatment, using parameters similar to that used in the grid laser treatment of diabetic retinopathy. Our results provide a description of baseline microglia behavior at rest and also how this behavior is regulated by focal injury. Taken together, our findings provide a perspective into the functional relevance of changing retinal microglia behavior in general and raise hypotheses about the mechanism underlying focal laser treatment for diabetic macular edema in particular.

MATERIALS AND METHODS

Experimental animals

CX3CR1$^{GFP/GFP}$ mice on a C57BL/6 background were obtained from The Jackson Laboratory (Bar Harbor, Maine). Heterozygous CX3CR1$^{+/GFP}$ were created by crossing CX3CR1$^{GFP/GFP}$ mice to wild type C57BL/6 mice, and housed and bred in NIH animal facilities. Experiments were conducted according to protocols approved by a local Institutional Animal Care and Use committee.

Vibratome sectioning and immunohistochemistry

Retinal tissue, fixed in 4% paraformaldehyde in 1× PBS, pH 7.3, was embedded in 7% agarose and sectioned with a vibrating microtome (Leica,VT1000S, Bannockburn, IL). Immunohistochemical staining with Griffonia simplicifolia IB4 (GSIB4) lectin, conjugated with Alexa 568 (1:100) to reveal vascular staining, 4',6-diamidino-2-phenylindole (DAPI)

(1:1000) to act as a nuclear marker (Invitrogen, Carlsbad, CA, USA), and Iba-1 (1:500) to label microglia (Wako Chemicals, Richmond, VA, USA) was performed.

Retinal explant wholemount preparation

Mice in age groups ranging from neonatal to 5 weeks of age were euthanized and enucleated. Eyecups were immediately immersed in ice-cold, oxygenated Ringer's solution (125mM NaCl, 5 mM KCl, 1.5mM CaCl$_2$, 0.75mM MgCl$_2$·6H$_2$0, 1.25mM NaH$_2$PO$_4$, 10mM D-Glucose, 20mM HEPES, pH 7.35–7.45). Retinas were dissected from the eyecups and then mounted on black Millipore filter paper (HABP045, Millipore, Billerica, MA) with the ganglion cell layer uppermost as described previously.[22]

Time-lapse confocal microscopy

Wholemount retina preparations were transferred to a stage-mounted, temperaturecontrolled (32°C) chamber (Bioptechs, Butler, PA) through which oxygenated Ringer's solution was continuously superfused (30–60 ml/hr). Tissue preparations were imaged using a confocal microscope (SP2; Leica, Exton, PA) and a 40x (0.80 numerical aperture) or 63x (0.90 numerical aperture) water-immersion objective. Multiplane Z series time-lapse images were collected at a 1024×1024 or 512×512 pixel resolution. Image stacks traversing volumes of interest were captured every 10 seconds.

Argon Laser Injury

Retinal tissue mounted on filter paper supports were placed perpendicular to the light-path of a slit-lamp mounted 532-nm photocoagulation laser (Iridex, Mountain View, CA). The aiming beam was focused on the plane of the retinal explant and 2 to 3 isolated focal laser burns were delivered, spaced >0.5 cm apart. Laser settings used were: power = 110 mW, duration = 100 ms, spot-size = 50 µm. Initial post-laser images were captured approximately 3 minutes following focal laser injury.

Image Processing

Image processing was performed using NIH ImageJ software. Two-dimensional (2D) representations of 3D microglial structures were created from maximum intensity projections in the z dimension, recursively aligned in the time dimension, and time-lapse movies created. Quantitative analysis of microglia processes were limited to those fully contained in the imaging space, avoiding focus changes artifacts that may be mistaken for structural changes. Mean microglial process velocities were calculated by tracking the ends of terminal processes over time using Plugin "MTrackJ" and quantitating the average rate of change of process displacement over the duration of the recording. Pixel-counting algorithms were used to quantify the two-dimensional area occupied by each cell at a single time point and across multiple time points from binarized z-projections of entire cellular arbors. Mean microglial migration velocities were calculated by tracking the centers of microglia soma over time and quantitating the average rate of soma displacement over the duration of the recording. Directional migration velocity was calculated from the change in distance of the cell soma relative to the center of the laser lesion (with a negative value representing movement towards the site injury) and dividing by the time interval of observation.

In order to characterize the polarization of cellular processes towards the site of laser injury for each individual cell, distances of all terminal processes were measured from the center of laser injury. A polarization coefficient, *P*, was defined:

$$P = (\overline{Dp - Ds})/Kd$$

where D_p = distance of process from center of laser injury, D_s = distance of soma from center of laser injury, and K_d = average diameter of microglia cells. A P of 1 represents a physical extreme of polarization where the tips of all cellular processes were located on one end of an arbor and the soma located on the other end, while a P of 0 represents a cell with the ends of terminal processes equally distributed between the half of the arbor closer to the injury and the other half further away. Polarization towards the laser injury is expressed as a negative value by this convention.

Statistical Analysis

The results were analyzed by two-tailed Student's t-test and are expressed as means ± SEM (unless otherwise indicated).

RESULTS

Distribution of microglia in the retina

We examined the distribution of GFP-labeled cells in the retina of young adult CX3CR1[+/GFP] mice between 4–5 weeks of age. Previous immunohistochemical studies of GFP-labeled cells in the cerebral cortex[23] and retina[14] of these transgenic animals have identified the cells as microglia based on the expression of cell-specific markers. We similarly verified in that all GFP-positive cells in the retina were also positive for Iba-1, a marker for microglia in the CNS (*data not shown*). GFP-labeled microglia in CX3CR1[+/GFP] mice had a similar distribution to that found in wild type mice.[6] In retinal cross-sections, the vast majority of microglia are located in the inner half of the retina and exhibit a horizontal laminar distribution extending from the nerve fiber layer (NFL) to the outer plexiform layer (OPL) (Fig. 1A), with only an occasional cell in the outer nuclear layer (ONL) or photoreceptor outer segments (OS). Examination of GFP-labeled microglia in retinal flat-mounts from CX3CR1[+/GFP] mice also revealed a regular distribution of microglia, with uniform spacing between adjacent cell soma of $73.1 \pm 2.1 \, \mu m$ (N = 55 cells in 5 animals) and ramified processes extending over "territories" (that we refer to as "arbors") that are spaced regularly and show little overlap (Fig. 1B).

Dynamic behavior of resting retinal microglia

To study the behavior of retinal microglia under uninjured conditions (the so-called "resting" microglia), we isolated living flat-mount retina explants from adult CX3CR1[+/GFP] mice. Acutely isolated explants were maintained in a temperature-controlled chamber through which oxygenated medium was perfused. Microglia in retinal explants had a typical "resting" morphology in which primary processes emerging from the cell body branch into smaller, terminal processes of variable lengths and shapes, often ending in bulbous tips (Fig. 2A). Time-lapse confocal microscopy was used to follow changes in structure and morphology of GFP-positive microglia under physiological conditions. We found that the processes of retinal microglia in the "resting" state are not static but highly dynamic, changing their structure at remarkably rapid rates [Supplementary online material, movie S1]. Both primary and terminal processes showed sustained changes in shape and length that occurred on the time-scale of seconds. In a single cell, these changes consisted of simultaneous extensions and retractions of existing processes, *de novo* formation of new processes, and process elimination (Fig. 2B) [Supplementary online material, movie S2].

Under resting conditions, process movements did not appear to be directed towards any particular orientation; processes extended in all directions, appearing to sample the surrounding extracellular space in a random fashion. Although the individual cell arbors are sometimes asymmetrical, there was no overall polarization in any one particular direction. The rapid process movements also did not result in significant changes to the overall area of the cell arbor

over the duration of recordings. Despite dynamic behavior on the level of microglial processes, the positions of cell bodies were relatively fixed, maintaing their spacing between neighboring cells.

Although the motile processes extend and retract rapidly in an apparently random and repeated fashion, processes of a single cell generally do not cross over each other's "territories", a phenomenon that also holds true for processes of the same cell. However, on occasion, the ends of terminal processes of adjacent cells can be seen extending to a common point to make transient contact before retracting (Fig. 3A) [Supplementary online material, movie S3]. In some cases, the ends of terminal processes from the same cell can also be seen making transient contact (Fig. 3B) [Supplementary online material, movie S4].

We also examined "resting" microglial behavior in developing retina from animals aged postnatal day (P)0 through P21. Developing microglia exhibited similar patterns of process motility (*data not shown*), indicating that dynamic microglia behavior is a property of both developing and mature systems.

Quantification of resting microglial dynamics

In order to quantitate the rate of process movement, we measured for each process the rate of change of displacement of its terminal end. The mean velocity of microglial processes of "resting" microglia was 5.44 ± 2.33 µm/min (mean ± standard deviation; n= 367 processes from 37 cells in 3 animals). These extremely rapid process movements have the effect of allowing the cell to sample the physical space in its "territory" repeatedly over a short period of time, and thus "occupy" a much larger cellular volume over time than it occupies at any single point in time (Fig. 4A and B). In 2-dimensional maximum intensity projections of time-lapse recordings, we computed a coverage factor that compared the total area occupied by a cellular arbor over a recording period of 8 minutes to that occupied at a single time point. This coverage factor was calculated to be approximately 315 ± 14.4 % (n=89 cells from 4 animals), indicating at least a 3-fold increase in the extent of space-filling achieved over 8 minutes when comparing a dynamic cell to an otherwise static cell. Despite these rapid changes, the overall sum of process additions and subtractions was balanced in all cells examined (n = 14 cells, from 5 animals), with the maintenance of overall size of the cell territory over time (Fig. 4C).

Morphological Response of Retinal Microglia to Focal Laser Injury

In addition to characterizing dynamic microglia behavior in the retina under resting conditions, we also examined how microglia behavior changes in response to focal retinal injury. Focal photocoagulative injury was administered to $CX3CR1^{+/GFP}$ retinal explants using an argon laser on a slit-lamp platform. The size of a typical laser burn was approximately 50–100 microns in diameter, similar to laser photocoagulation delivered in the treatment of diabetic macular edema (Fig. 5A). Higher magnification imaging showed that within 5 minutes post-laser, microglia in the immediate vicinity (<500 µm) of the laser spot directed processes preferentially towards the injury site. This tropism of processes towards the center of injury became more marked with increasing time post-injury. Microglia progressively extended new processes towards the laser lesion, while withdrawing processes on the side of the cell furthest from the injury (Fig. 5B and C) [Supplementary online material, movie S5].

To reflect the directed polarity of cellular morphologies, we computed a polarity coefficient that takes into account the distribution of cellular processes on either side of the cell with respect to the location of focal injury. Figure 5C illustrates an example of a microglia cell with increasing polarization of its structure after laser injury. The increased polarization of this cell over time is qualitatively apparent by its changing morphology and can be quantified by an increasingly negative polarity coefficient (Fig. 5C, bottom left).

We observed that, in addition to increasing polarity, post-injury microglial morphologies also became progressively less branched with an overall decrease in both primary and terminal processes (Figure 5C, bottom right). As time progressed, most microglia within a 500-micron radius of the injury extended fewer but longer processes toward the injury site. Microglia generally became significantly polarized ≥30 minutes after injury (Figure 5D) with fewer branched structures (Figure 5E). The extent of polarization, however, did not vary significantly with distance from the center of injury within the 500µm radius (data not shown).

Dynamic Response of Retinal Microglia Processes to Focal Laser Injury

Unlike resting microglia, which maintain stationary cell body positions despite dynamic process motility, post-laser injury microglia acquire a migratory capacity as demonstrated detectable displacement of their cell somata during a recording. These cellular migrations were significantly slower than the rate of process movements, averaging 0.45 ± 0.48 µm/min (mean ± standard deviation, n=150 cells from 11 recordings in 5 animals) (Fig 6A). Not all microglia were migratory following laser injury, and the rate of migration was also variable between cells [Supplementary Online Material, movie S6 and Supplementary Online Material, movie S7]. These migratory microglia retain their highly ramified morphologies and were capable of restructuring their processes and translocating through tissue at the same time. Occasionally, microglia with activated, amoeboid morphologies were seen migrating at a higher than average rate (Fig. 6B) [Supplementary Online Material, movie S8]. The movements of these amoeboid cells were not included in the calculation of average migration velocity. Migration velocity varied with soma-to-laser injury distance, decreasing significantly (p<0.02) for cells outside a 400µm radius of the lesion (Fig. 6C). Although migratory movements in some cells were in the direction of the laser lesion, computations of migrational directionality on the whole did not reveal a consistent tropism towards or away from the site of injury over the relatively short time scale of the recordings (*data not shown*).

Quantitation of process motility also revealed that average process velocity was markedly elevated after laser injury, measuring 9.06 ± 3.37 µm/min (mean ± standard deviation, n=363 processes from 99 cells in 3 animals) (Fig. 6C), or about 167% of that in "resting" microglia. The effect of increased motility also translated into an increased microglial coverage of the surrounding intercellular space; maximum intensity projections over 8 minutes of recording showed a coverage factor of 384±12%, significantly higher than the 315% calculated for resting microglia.

DISCUSSION

We have employed an intact retinal explant *ex vivo* system to examine the nature of retinal microglial process dynamics. Unlike acute brain slice preparations where the slicing procedure results in extensive tissue damage in close proximity to resident microglia, retinal wholemount preparations isolate retinal tissue as an intact sheet with preservation of neuronal circuitry and retinal vasculature, thus maintaining neuronal connectivity and cellular behavior, as demonstrated by other experiments employing this preparation.[24, 25] Retinal microglia in wholemount preparations were observed to retain their ramified morphology and laminar distribution many hours after acute isolation and did not progress through morphological changes typical of microglia activation seen in brain slice preparations.[26] GFP-labeled retinal microglia in similar transgenic mice have been previously imaged *in vivo* using confocal scanning laser ophthalmoscopy in which microglia distribution and migration were monitored after laser injury over hours to days.[21, 27] Individual cellular morphologies and processes could not however be visualized and followed. Our imaging system affords a higher spatial and temporal resolution that complements those observations by visualizing microglial behavior continuously on the level of the individual cell and the individual process.

Our results show that so-called "resting" retinal microglia show a rapid dynamism in their processes that is continuous and sustained but is however unaccompanied by cellular migration on the level of the soma. These process movements appear random, involve both primary and terminal branches of the cellular arbor, and occur in all directions. Extrapolation of process movements over time reveal that resting retinal microglia are capable of sampling their entire extracellular space repeatedly over a time-scale of minutes. These observations support an endogenous surveillance function for rapid process motility in resting microglia. Our observations of transient, coordinated contact between terminal microglial processes among otherwise random patterns of motility in addition suggest that process dynamics may also serve to exchange signals between neighboring microglia. These communications may explain why retinal microglia distribution in the neural parenchyma occurs in a laminar, tiled fashion with little overlap between arbors and explain how seemingly random movements are limited to each cellular arbor's territory. Taken together, our observations indicate that rapid and continuous microglial coverage of the inner retina is a constitutive and constant physiological property of the intact and healthy retina.

Our observations of the behavior of resting retinal microglia resemble those documented for microglia in the cerebral cortex[19, 20] and other CX3CR1-positive immune cells in visceral organs[28, 29] in terms of pattern and nature. The average velocity of moving microglial process was considerably higher in the retina than cerebral cortex (5.4±2.3 µm/min versus 1.5±0.1 µm/min).[20] While the nature of the two systems are clearly different (*ex vivo* retinal explant versus *in vivo* in an anesthetized animal), further investigation of the effects of neuronal activity or metabolic rate on microglial dynamics may be insightful to the evaluation of resting microglia behavior across specialized areas of the CNS.

The function of retinal microglia process dynamics may also be illuminated by evaluation of microglial response to focal injury. We found that process dynamics were altered post-injury in a number of significant ways. First, average process velocity in the vicinity of the laser burn increased significantly by 67% in the first hour after laser injury. Second, the process movements changed from a state without orientation to one clearly directed towards the laser lesion. Also, the overall balance between process additions and eliminations was shifted to result in a polarized and simplified cellular arbor. Lastly, some retinal microglia acquired a post-injury migratory phenotype that allowed translocation through the retina while maintaining rapid process motility. The migratory behavior of polarized retinal microglia was not demonstrably directed towards the laser lesion, though there may be a net accumulation of microglia in the vicinity of the laser lesion over longer periods of time[21]. The migration exhibited by ramified, polarized microglia appeared to be distinct from the rapid locomotion of activated, amoeboid microglia lacking a ramified morphology. The latter were seen infrequently post-laser in this preparation while they can be widely found in brain slice preparations.[26] These microglia in post-laser retina probably represent a smaller subset of reactive microglia that have been activated to a greater degree and have transitioned to an amoeboid, highly migratory morphology. This phenotypic diversity in retinal microglia after injury reflect a similar diversity of potential microglial responses that are likely to vary with injury intensity and dose, and may underlie different aspects of tissue response[2].

The directed and distance-dependent nature of microglial response to laser injury suggest a role for diffusible chemoattractant signals originating from the injury site that upregulate process motility, reorient microglial morphology, and confer migratory behavior. Other studies have indicated that extracellular ATP, acting through P2Y receptors, may be involved in microglial response to injury.[19, 30] In this study we have used laser injury parameters that simulate retinal laser burns delivered in the treatment of diabetic macular edema. We speculate that the changing behavior of retinal microglia from a resting, stationary state to a polarized, migratory state with increasingly rapid surveying movements may underlie tissue responses

after focal laser treatment in retinal disease. Retinal microglia may exist in a variety of activity states,[2] and may shift from a "resting" to an "alerted" state after local injury. "Alerted" microglia may release neurotrophic factors and inflammatory mediators that exert beneficial vasculoprotective and neuroprotective effects that underlie the therapeutic benefit seen in focal laser treatment for diabetic macular edema.[31] Future investigations of factors that regulate microglial behavior in both in normal retina and in models of retinal disease may further clarify what endogeneous roles retinal microglia play under normal conditions and how they may contribute to the pathogenesis of retinal disorders.

Supplementary Material

Refer to Web version on PubMed Central for supplementary material.

Acknowledgements

REFERENCES

1. Kreutzberg GW. Microglia: a sensor for pathological events in the CNS. Trends Neurosci 1996;19:312–318. [PubMed: 8843599]

2. Hanisch UK, Kettenmann H. Microglia: active sensor and versatile effector cells in the normal and pathologic brain. Nat Neurosci 2007;10:1387–1394. [PubMed: 17965659]

3. Kim SU, de Vellis J. Microglia in health and disease. J Neurosci Res 2005;81:302–313. [PubMed: 15954124]

4. Block ML, Zecca L, Hong JS. Microglia-mediated neurotoxicity: uncovering the molecular mechanisms. Nat Rev Neurosci 2007;8:57–69. [PubMed: 17180163]

5. Chen L, Yang P, Kijlstra A. Distribution, markers, and functions of retinal microglia. Ocul Immunol Inflamm 2002;10:27–39. [PubMed: 12461701]

6. Santos AM, Calvente R, Tassi M, et al. Embryonic and postnatal development of microglial cells in the mouse retina. J Comp Neurol 2008;506:224–239. [PubMed: 18022954]

7. Schuetz E, Thanos S. Microglia-targeted pharmacotherapy in retinal neurodegenerative diseases. Curr Drug Targets 2004;5:619–627. [PubMed: 15473251]

8. Langmann T. Microglia activation in retinal degeneration. J Leukoc Biol 2007;81:1345–1351. [PubMed: 17405851]

9. Lewis GP, Sethi CS, Carter KM, Charteris DG, Fisher SK. Microglial cell activation following retinal detachment: a comparison between species. Mol Vis 2005;11:491–500. [PubMed: 16052164]

10. Gupta N, Brown KE, Milam AH. Activated microglia in human retinitis pigmentosa, late-onset retinal degeneration, and age-related macular degeneration. Exp Eye Res 2003;76:463–471. [PubMed: 12634111]

11. Neufeld AH. Microglia in the optic nerve head and the region of parapapillary chorioretinal atrophy in glaucoma. Arch Ophthalmol 1999;117:1050–1056. [PubMed: 10448748]

12. Zeng HY, Green WR, Tso MO. Microglial activation in human diabetic retinopathy. Arch Ophthalmol 2008;126:227–232. [PubMed: 18268214]

13. Zeiss CJ, Johnson EA. Proliferation of microglia, but not photoreceptors, in the outer nuclear layer of the rd-1 mouse. Invest Ophthalmol Vis Sci 2004;45:971–976. [PubMed: 14985319]

14. Combadiere C, Feumi C, Raoul W, et al. CX3CR1-dependent subretinal microglia cell accumulation is associated with cardinal features of age-related macular degeneration. J Clin Invest 2007;117:2920–2928. [PubMed: 17909628]

15. Tuo J, Bojanowski CM, Zhou M, et al. Murine ccl2/cx3cr1 deficiency results in retinal lesions mimicking human age-related macular degeneration. Invest Ophthalmol Vis Sci 2007;48:3827–3836. [PubMed: 17652758]

16. Gaucher D, Chiappore JA, Paques M, et al. Microglial changes occur without neural cell death in diabetic retinopathy. Vision Res 2007;47:612–623. [PubMed: 17267004]

17. Eder C. Regulation of microglial behavior by ion channel activity. J Neurosci Res 2005;81:314–321. [PubMed: 15929071]

18. Garden GA, Moller T. Microglia biology in health and disease. J Neuroimmune Pharmacol 2006;1:127–137. [PubMed: 18040779]

19. Davalos D, Grutzendler J, Yang G, et al. ATP mediates rapid microglial response to local brain injury in vivo. Nat Neurosci 2005;8:752–758. [PubMed: 15895084]

20. Nimmerjahn A, Kirchhoff F, Helmchen F. Resting microglial cells are highly dynamic surveillants of brain parenchyma in vivo. Science 2005;308:1314–1318. [PubMed: 15831717]

21. Eter N, Engel D, Meyer L, et al. In vivo visualization of dendritic cells, macrophages and microglial cells responding to laser-induced damage in the fundus of the eye. Invest Ophthalmol Vis Sci. 2008

22. Wong WT, Sanes JR, Wong RO. Developmentally regulated spontaneous activity in the embryonic chick retina. J Neurosci 1998;18:8839–8852. [PubMed: 9786990]

23. Cardona AE, Pioro EP, Sasse ME, et al. Control of microglial neurotoxicity by the fractalkine receptor. Nat Neurosci 2006;9:917–924. [PubMed: 16732273]

24. Wong RO, Chernjavsky A, Smith SJ, Shatz CJ. Early functional neural networks in the developing retina. Nature 1995;374:716–718. [PubMed: 7715725]

25. Wong WT, Faulkner-Jones BE, Sanes JR, Wong RO. Rapid dendritic remodeling in the developing retina: dependence on neurotransmission and reciprocal regulation by Rac and Rho. J Neurosci 2000;20:5024–5036. [PubMed: 10864960]

26. Stence N, Waite M, Dailey ME. Dynamics of microglial activation: a confocal time-lapse analysis in hippocampal slices. Glia 2001;33:256–266. [PubMed: 11241743]

27. Paques M, Simonutti M, Roux MJ, et al. High resolution fundus imaging by confocal scanning laser ophthalmoscopy in the mouse. Vision Res 2006;46:1336–1345. [PubMed: 16289196]

28. Auffray C, Fogg D, Garfa M, et al. Monitoring of blood vessels and tissues by a population of monocytes with patrolling behavior. Science 2007;317:666–670. [PubMed: 17673663]

29. Soos TJ, Sims TN, Barisoni L, et al. CX3CR1+ interstitial dendritic cells form a contiguous network throughout the entire kidney. KidneyInternational 2006;70:591–596.

30. Kurpius D, Nolley EP, Dailey ME. Purines induce directed migration and rapid homing of microglia to injured pyramidal neurons in developing hippocampus. Glia 2007;55:873–884. [PubMed: 17405148]

31. Early photocoagulation for diabetic retinopathy. ETDRS report number 9. Early Treatment Diabetic Retinopathy Study Research Group. Ophthalmology 1991;98:766–785. [PubMed: 2062512]
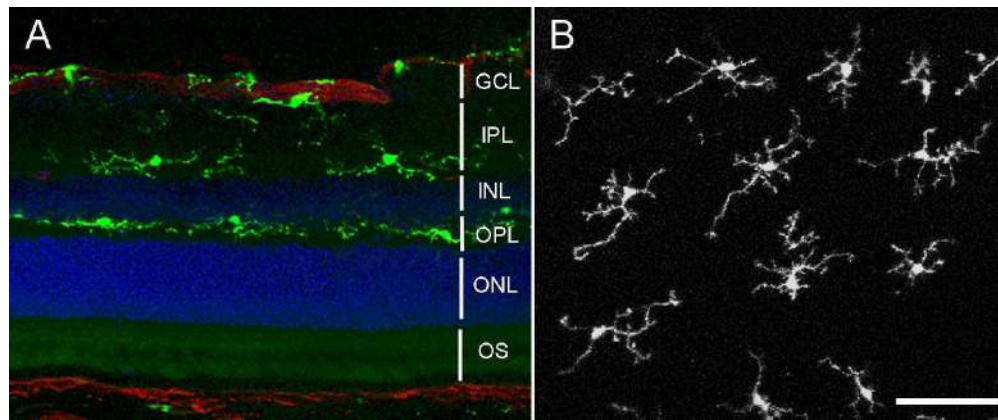
Figure 1. Distribution of microglia in the retina
(A) Agarose-embedded sections showing distribution of GFP-positive microglia (*in green*) in CX3CR1$^{+/GFP}$ animals in the inner retina, primarily in the ganglion cell layer (GCL), inner plexiform layer (IPL), and outer plexiform layer (OPL). Nuclei were labeled with DAPI (blue), and vessels with GSIB4 lectin (red) **(B)** Confocal image from a retinal wholemount explant showing the distribution of ramified, GFPpositive microglia in the outer plexiform layer. (Scale bar = 50 µm) INL = inner nuclear layer, ONL = outer nuclear layer, OS = photoreceptor outer segments.
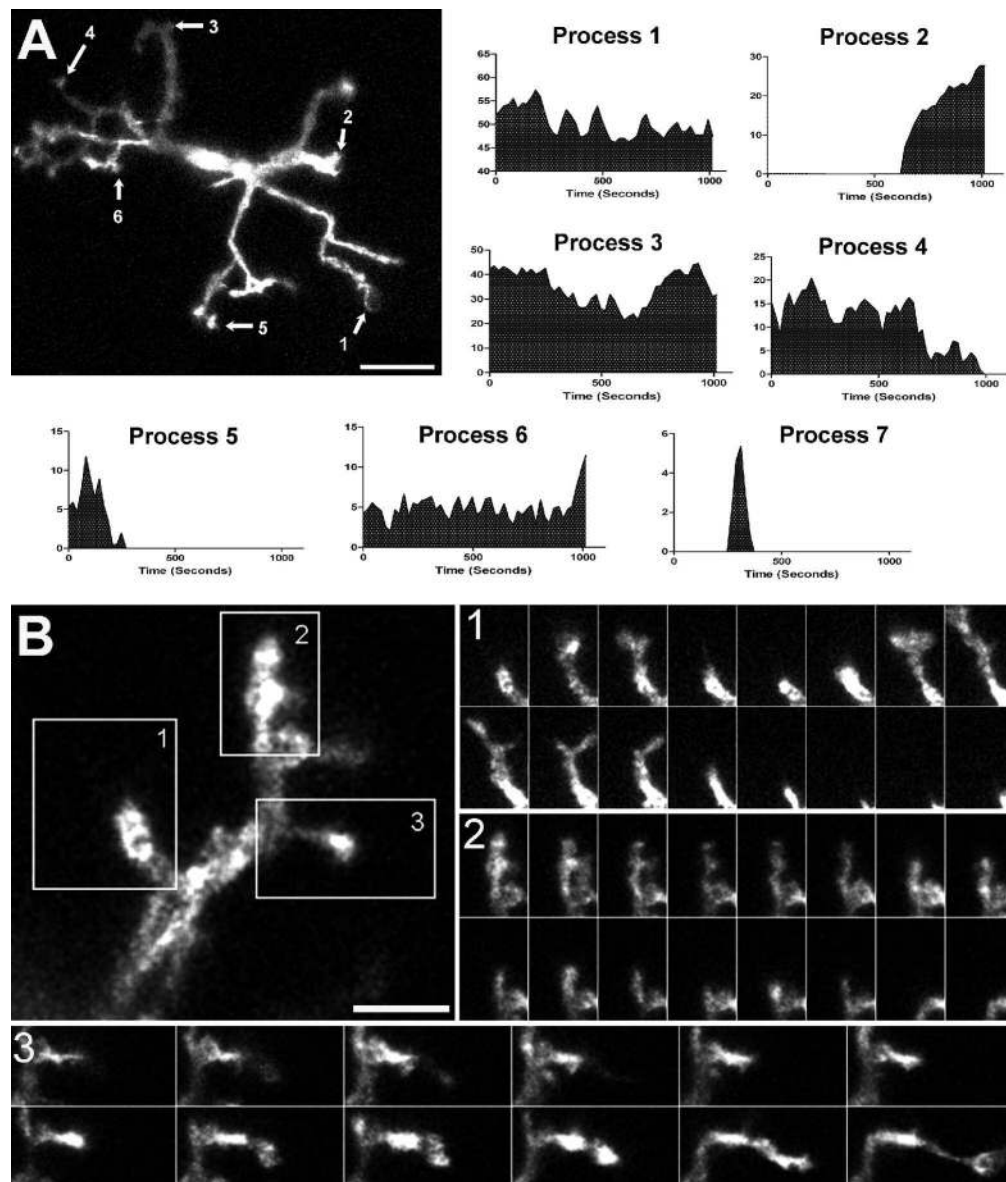
Figure 2. Resting retinal microglia show marked process motility
(A) Microglial cell in a CX3CR1$^{+/GFP}$ mouse retina imaged with time-lapse confocal microscopy. Length-versus-time profiles for each cellular process (indicated by arrows and numbered) demonstrate extension and retraction movements. Scale bar = 50µm. Process 7 was transient with a short half-time (not located on figure) [Supplementary online material, movie S1] **(B)** High-magnification confocal image of a single microglial process bearing multiple tertiary terminal processes. Image series in insets (taken 10s apart) show progressive structural changes in existing processes, *de novo* initiation of processes, and complete elimination of existing processes. Scale bar = 5µm. [Supplementary online material, movie S2]
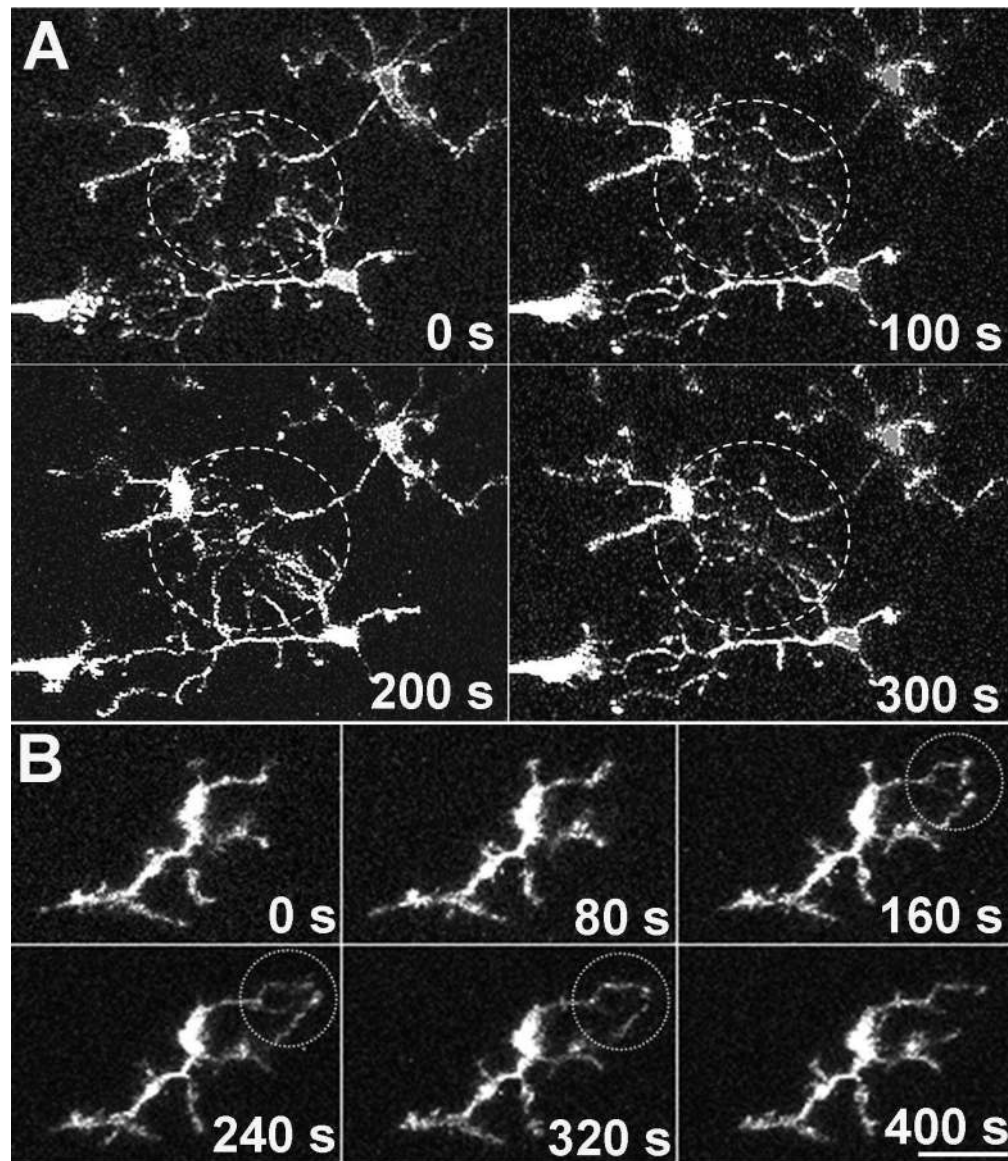
Figure 3. Terminal ends of microglial processes make occasional transient contact with each other
(A) Neighboring microglia progressively extend their processes to meet transiently at a common point (circle) before disengaging and retracting. [Supplementary online material, movie S3] **(B)** A single cell extends adjacent terminal processes whose tips meet transiently at a single point (circle). [Supplementary online material, movie S4] Scale bar = 20µm.
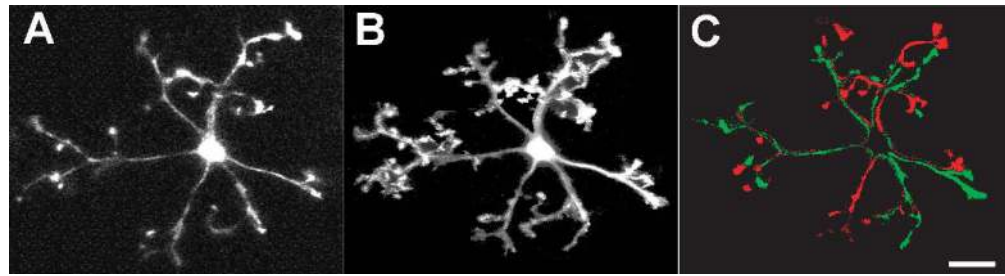
Figure 4. Distribution of structural changes over the entire microglia cell arbor
Comparison of the area occupied by a microglia cell at one point in time **(A)** with the area occupied by the same cell over 500s (maximum z-projection of 50 time-lapse images, captured 10s apart **(B)** demonstrates the ability of dynamic cellular processes to sample a large volume of extracellular space. **(C)** Subtraction image between confocal images captured at time = 0s and at t = 500s shows that the extent of process additions (in green) are balanced by the extent of process retractions (in red). Scale bar = 20μm.
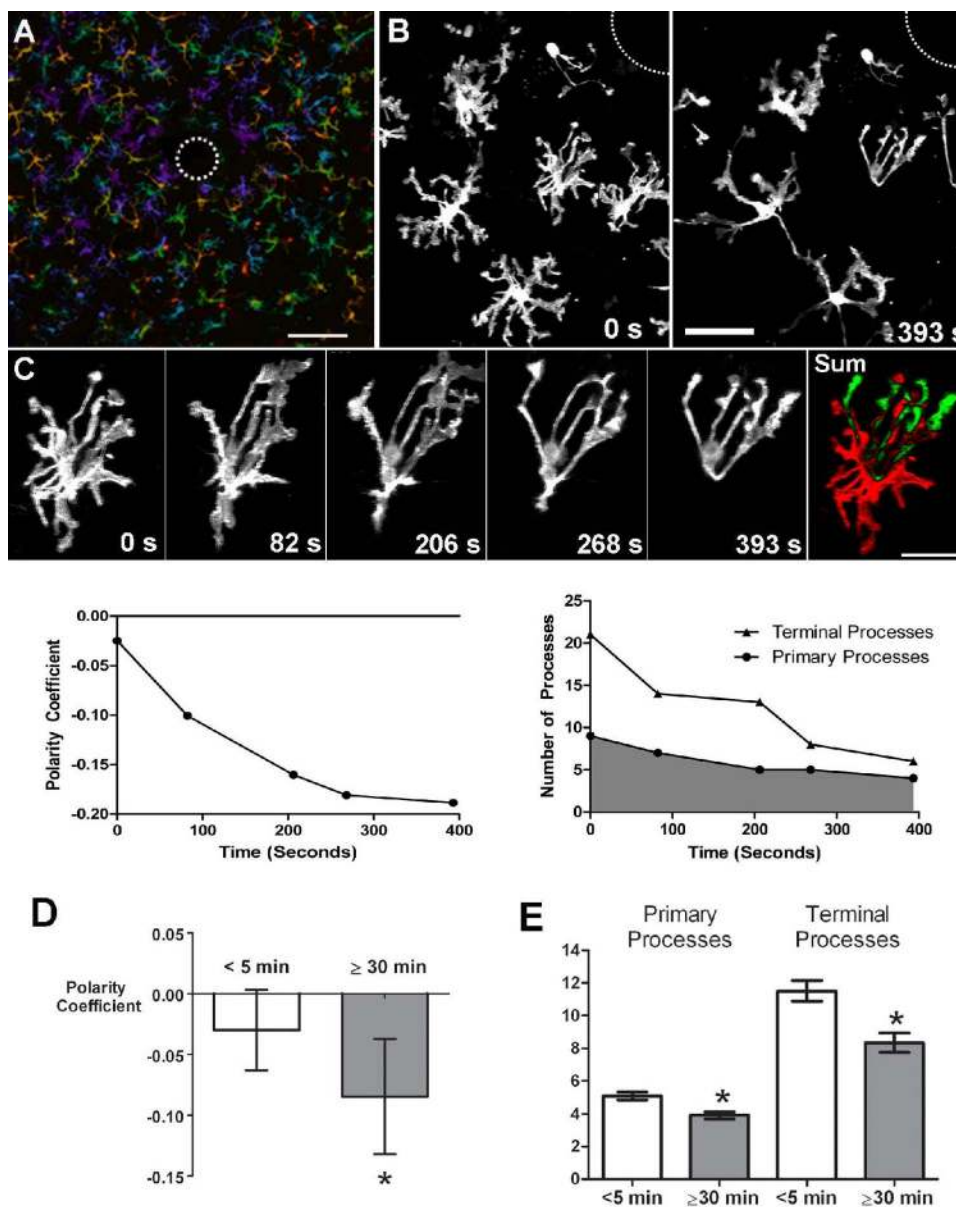
Figure 5. Morphological responses of microglia to focal laser injury
(A) Low magnification (20X) view of microglia in the vicinity of a focal laser burn (dotted circle) with colors representing depth in the Z-direction (purple=superficial and red=deep). Scale bar = 100µm. (B) Higher magnification of microglia at the edge of the laser burn (dotted circle) immediately (*left*) and 393s after (*right*) laser injury. Scale bar = 30 µm (C) Cell from inset in (*B*) showing progressive morphological change in response to laser injury. [Supplementary online material, movie S5] Subtraction image (*right*) between the initial and final images demonstrate that processes are extended in the direction of the laser burn (in green) and withdrawn on the opposite side of the cell (in red). Scale bar = 20µm. Graph of polarity coefficient vs. time after laser (*lower left*) demonstrates increasing polarization of the cell towards the laser burn with time. Graph of process number vs. time (*lower right*) shows decreasing number of primary and terminal processes after laser injury. (D) Polarity coefficients of multiple microglial cells immediately post-laser injury (0 to 5 min) and after a

waiting period (30–70 minutes). Error bars indicate 95% confidence intervals. Cells were slightly but not significantly polarized <5 min after injury but became significantly polarized ($p < 0.05$) after 30 min. **(E)** Numbers of primary and terminal processes per cell are significantly reduced after 30 minutes post-laser injury (asterisks indicate $p < 0.05$). Analysis of (*D*) and (*E*) based on 153 cells from 24 time-lapse recordings in 6 animals.
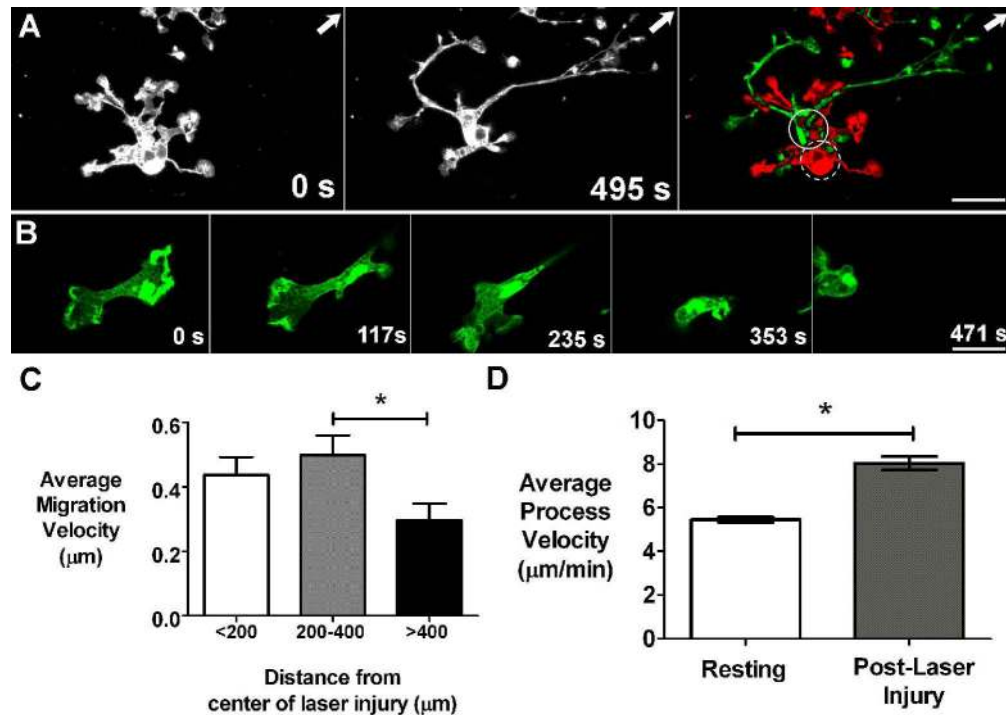
Figure 6. Dynamic behavior of microglia after focal laser injury
(**A**) Microglia cell in the vicinity of laser burn (arrow indicates location of laser burn outside image field) soon after laser injury (t = 0s) and approximately 8 minutes afterwards (t = 495s). Subtraction image *(right)* between these 2 time-points shows displacement of cell body position (dashed and solid circles indicate soma position at 0s and 495s respectively) in addition to a progressive extension of processes towards the laser burn. [Supplementary online material, movie S6] (**B**) An amoeboid microglia is seen near the laser injury site and migrates across the imaging field. [Supplementary online material, movie S8] Scale bars = 15 µm. (**C**) Average migration velocity of ramified microglia at different distances from the center of laser injury. The average rates of cellular migration is similar between cells up to 400 microns away from the center of laser injury, but cellular migration decreases significantly with distances greater than 400 microns from the injury site (asterisk indicates p < 0.05). (**D**) Average velocity of microglia processes after laser injury (n = 363 processes from 99 cells from 12 recordings in 3 animals) increased significantly (p <0.05) compared to that in the resting state (n = 363 processes from 37 cells from 7 recordings in 3 animals).